



Published in final edited form as:

ACS Nano. 2017 July 25; 11(7): 7424–7430. doi:10.1021/acsnano.7b03711.

Dual mode mass spectrometric imaging for determination of *in vivo* stability of nanoparticle monolayers

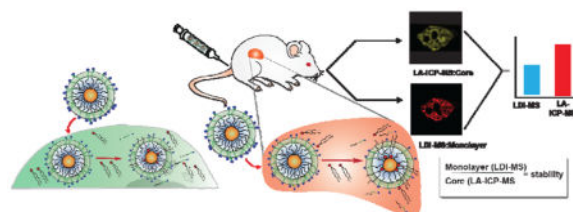
S. Gokhan Elci, Gulen Yesilbag Tonga, Bo Yan, Sung Tae Kim, Chang Soo Kim, Ying Jiang, Krishnendu Saha, Daniel F. Moyano, Alyssa L. M. Marsico, Vincent M. Rotello, and Richard W. Vachet*

Department of Chemistry, University of Massachusetts, 710 North Pleasant Street, Amherst, MA, 01003

Abstract

Effective correlation of the *in vitro* and *in vivo* stability of nanoparticle-based platforms is a key challenge in their translation into the clinic. Here, we describe a novel dual imaging method that site-specifically reports the stability of monolayer-functionalized nanoparticles *in vivo*. This approach uses laser ablation inductively-coupled plasma mass spectrometry (LA-ICP-MS) imaging to monitor the distributions of the nanoparticle core material and laser desorption/ionization mass spectrometry (LDI-MS) imaging to report on the monolayers on the nanoparticles. Quantitative comparison of the images reveals nanoparticle stability at the organ and sub-organ level. The stability of particles observed in the spleen was location-dependent and qualitatively similar to *in vitro* studies. In contrast, *in vivo* stability of the nanoparticles in the liver differed dramatically from *in vitro* studies, demonstrating the importance of *in vivo* assessment of nanoparticle stability.

Graphical Abstract



Keywords

Nanoparticles; dual imaging; LDI-MS; LA-ICP-MS; *in vivo* monolayer stability

Nanoparticles (NPs) offer key delivery^{1,2} and imaging platforms^{3,4} for biological applications.^{5,6} NPs provide unique physico-chemical attributes with potential to overcome challenges including biological barriers,⁷ rapid clearance,^{8,9} and ineffective delivery of the cargo to the target.^{10,11} A wide range of therapeutic payloads ranging from small molecules to proteins and nucleic acids have been conjugated to NPs to provide delivery systems.^{12,13}

*rwvachet@chem.umass.edu.

These systems have shown great promise in pre-clinical studies,^{14,15,16,17} and in the clinic,^{18,19} including AuroLase and Magnablate.^{20–23}

Effective biomedical application of nanomaterials requires effective understanding and correlation of *in vitro* and *in vivo* behavior.²⁴ In addition to physical parameters such as size and shape,^{25,26} dynamic changes in the NP surface or structure in the blood stream or within organs will change their behavior.^{27,28} This remodeling can dictate NP fate by altering cellular uptake,¹⁵ corona formation,^{16–18} biodistribution,¹⁹ interactions with biomolecules,²⁰ pharmacokinetics,²⁹ and pharmacodynamics parameters.^{30,31} Current strategies for tracking NPs generally focus on the quantification of the NP core^{32,33} rather than considering surface stability.

Here, we describe a dual-mode mass spectrometric imaging approach that provides site-specific quantitative information on inorganic NP monolayer stability.^{3,34} We use laser ablation inductively-coupled plasma mass spectrometry (LA-ICP-MS) imaging³⁵ to track the distributions of NP core and laser desorption/ionization (LDI) MS imaging^{36,37} to track the distributions of ligands that are still bound to the NP core. Comparison of the two images indicates the extent to which the NPs monolayers retain their integrity. Using this strategy, we show how NP stability dramatically diverges in different organs and sub-organs and simultaneously establish that there can be varying stability profiles for NPs *in vitro* and *in vivo*.

Five different AuNPs (Figure 1(a), AuNPs 1–5) with the same core size (2 nm) but different surface monolayers were used to determine the ability of the dual mode imaging approach to report on monolayer stability. These ligands possess four functional segments: 1) a mono or dithiol group for anchoring ligands to the NP surface,³⁸ 2) a hydrophobic alkane group for core stability,³⁹ 3) a tetra(ethylene glycol) (TEG) group for biocompatibility,⁴⁰ and 4) a variable head group for chemical diversity.⁴¹ The chemical identity of these layers plays a role in the stability of the monolayer.^{34,3} Dithiol groups offer a more stable anchor to the gold core than mono thiols; longer alkane chain lengths better protect the gold core than shorter chains; and the presence of the TEG group has been shown to impart greater NP stability.³⁴ When NPs like those shown in Figure 1 are injected into mice, their biodistribution typically feature high levels of accumulation in the liver and spleen, two important organs of reticulo-endothelial system (RES).^{42,43} Due to the high accumulation of administered NPs in the RES system (30–99%),^{44,45} we investigated the changes in AuNPs in the spleen and liver by tracking the monolayer stability using our combined imaging approach. The AuNPs (Figure 1) were injected into mice intravenously (see details in the SI), and after fixed time points the mice were sacrificed and their organs were collected.

We first investigated the stability of AuNPs in the spleen of mice injected with AuNP 1, with the expectation that the loss of monolayer in this organ would be slower than for the liver due to lower endogenous thiol levels.⁴⁶ Imaging of the spleen 24 h after injection (Figure 2a) provides preliminary evidence for retention of ligands of AuNP 1, as the signal associated with the monolayer ligand in the LDI-MS image (Figure 2b) arises from only ligands attached to the core.³⁷ As expected, this signal co-localizes with the signal from Au in the LA-ICP-MS image (Figure 2c), indicating the presence of AuNPs with intact monolayers.

We then investigated the spleen stability of AuNPs at different time points (4, 24, and 48 h) after their injection into the mice. AuNPs 1, 2, and 3 were simultaneously injected, and LDI-MS images for each NP's monolayer signal were generated. We predicted that the ligand signal in the LDI-MS images would decrease after longer time points as the AuNPs are degraded over time. As expected, LDI-MS images of the spleen showed a decrease in the monolayer signal for each AuNP over time (Figure 2d). An evaluation of the ion intensities in these images (Figure 2e), after normalizing for the size of the tissue, confirms this observation and further indicates that the signal drops for each AuNP is similar. In contrast, the Au distributions in the spleen, as determined by LA-ICP-MS imaging, indicate that the Au amounts remain essentially constant when the data is normalized for mouse-to-mouse variations (e.g. Figure S1 and S2). Taken together, comparison of the LDI-MS and LA-ICP-MS imaging results reveal that ~50% of the monolayer stability is lost in the spleen over a 48 h period, with headgroup structure playing a rather small role in determining particle stability.

Studies using AuNPs 1–3 (Figure 2) show that these NPs have similar stability. The ability of the system to determine differential monolayer stability was probed using AuNPs 1 and 4; previous *in vitro* findings showed that incorporating TEG moieties in the monolayer provides enhanced stability in cells.³⁴ We first compared the LDI-MS behavior of these two ligand systems, finding that they had similar ionization efficiencies (Figure S3). To best compare the two sets of images, we imaged two sets of tissues that had similar total gold amounts based on ICP-MS measurements of tissue homogenates (Figure S4). The LDI-MS signals (shown in green) are qualitatively brighter for AuNP 1 (Figure 3a), indicating higher ligand stability for AuNP 1 relative to AuNP 4. A more quantitative comparison was made by summing the ion abundances in each pixel and dividing this value by the total area of the image, while also correcting for the slight differences in ionization efficiencies of the two monolayers (Figure 3b). From such an analysis, both AuNPs are found to have similar abundances per unit area in the LA-ICP-MS images but quite different ion abundances are observed per unit area in the LDI-MS images (Figure 3b). From these studies we can conclude that AuNP 1 is essentially unchanged in the spleen, whereas ~60% of the monolayer of AuNP4 was degraded. These outcomes correlate well with our previous *in vitro* results,³⁴ and provide a strong demonstration of the importance of monolayer structure on *in vivo* stability.

The use of imaging tools allows the monitoring of NP stability across individual organs.⁴⁷ LDI-MS and LA-ICP-MS images of spleens from mice injected with AuNP 1 and 4 were compared to determine stability differences at the sub-organ level. H&E staining and Fe images from the LA-ICP-MS experiments were used to identify the three primary regions of the spleen: red pulp, white pulp, and marginal zone (Figure 4).⁴⁷ For the analysis, the average ligand and Au signals for each spleen region were determined separately, as described in the SI, and then a stability factor for each AuNP was calculated from the ratio of the ligand signal to Au signal (Figures S5, S6, S7, and Table S4). The calculated stability factor indicates that AuNP 1 and AuNP 4 have similar stability in the red pulp, while AuNP 1 is slightly more stable in the white pulp. Interestingly, AuNP 1 is significantly more stable than AuNP4 in the marginal zone (Table S4). This increased level of degradation suggests an increased level of biogenic thiols in the marginal zone relative to the rest of the spleen, a

property that to our knowledge has been suggested,^{48,49} but has not been experimentally observed.

Having established the ability of the dual imaging strategy to determine stability in the spleen, we next examined the stability of NPs in the liver. Mice were injected with AuNP 1, and after 24 h were sacrificed. Slices from the liver were then imaged by LDI-MS for the ligand and LA-ICP-MS for Au. As expected, LA-ICP-MS indicates high levels of Au in the liver (Figure 5a). In contrast, LDI-MS shows no ligand signal, indicating complete degradation of the AuNP monolayer. This outcome is surprising because previous studies showed that AuNPs with similar ligands were reasonably stable (~70% monolayer retention) for *in vitro* studies using liver (HepG2) cells.³⁴ In a control experiment, AuNPs that were added to liver tissue slices gave rise to significant ligand ion signal (Figure S8), eliminating the possibility that LDI-MS does not work in liver tissue.

Given the total degradation of the monolayer observed with even our most stable monothiol ligand, we performed a further 24 h trial using dithiol-functionalized AuNP 5 (Figure 1). Previous *in vitro* studies showed complete (100%) retention of the monolayer of AuNP 5 in HepG2 liver cells;³⁴ given this outcome we expected similar behavior *in vivo*. In stark contrast to the *in vitro* studies, however, no ligand is observed by LDI-MS (Figure 5b). These studies indicate a remarkable difference between *in vitro* and *in vivo* stability, a key observation that calls into question the utility of *in vitro* studies to predict *in vivo* behavior.^{50,51} While the mechanism for enhanced degradation *in vivo* is unknown, the difference in behavior can be explained at least in part by increased levels of biogenic thiols *in vivo* arising from the complex network of inter-related cells including hepatocytes, Kupffer cells, macrophages, and immune cells (dendritic cells, natural killer cells, and lymphocytes) found in the liver.⁴⁴

In summary, we have developed a dual mode imaging approach that combines LA-ICP-MS and LDI-MS imaging to quantify AuNP monolayer stability *in vivo*. This technique provides a tool for quantifying particle stability *in vivo*, producing results dramatically different than those predicted from *in vitro* studies. Imaging studies of the liver revealed stark differences between *in vitro* and *in vivo* behavior. Even NPs that were completely stable in liver cells *in vitro* were completely degraded *in vivo*. The resolution of the techniques enabled determination of the sub-organ stability of the particles. These studies indicate marked differences in AuNP stability at different locations in the spleen, indicating that this dual-imaging strategy has the capability of providing unprecedented granularity of our understanding of the pharmacodynamic properties of nanomaterials. Taken together, these results indicate that *in vitro* systems have unexpected limitations in predicting *in vivo* pharmacodynamics, an issue that we will pursue in future imaging studies.

Supplementary Material

Refer to Web version on PubMed Central for supplementary material.

Acknowledgments

This research was supported by the NIH (GM GM077173, EB022641, VR) and the NSF (Center for Hierarchical Manufacturing, CMMI-1025020 and CHE-1506725).

References

1. Rana S, Bajaj A, Mout R, Rotello VM. Monolayer coated gold nanoparticles for delivery applications. *Adv Drug Deliver Rev.* 2012; 64:200–216.
2. Verma A, Uzun O, Hu Y, Han HS, Watson N, Chen S, Irvine DJ, Stellacci F. Surface-structure-regulated cell-membrane penetration by monolayer-protected nanoparticles. *Nat Mater.* 2008; 7:588–595. [PubMed: 18500347]
3. Zhu ZJ, Yeh YC, Tang R, Yan B, Tamayo J, Vachet RW, Rotello VM. Stability of quantum dots in live cells. *Nat Chem.* 2011; 3:963–968. [PubMed: 22109277]
4. Park Y II, Lee KT, Suh YD, Hyeon T. Upconverting nanoparticles: a versatile platform for wide-field two-photon microscopy and multi-modal in vivo imaging. *Chem Soc Rev.* 2015; 44:1302–1317. [PubMed: 25042637]
5. Cully M. Nanoparticles improve profile of molecularly targeted cancer drug. *Nat Rev Drug Discov.* 2016; 15:231. [PubMed: 27032829]
6. Vasudevanpillai B. Chemical modifications and bioconjugate reactions of nanomaterials for sensing, imaging, drug delivery and therapy. *Chem Soc Rev.* 2014; 43:744–764. [PubMed: 24220322]
7. Blanco E, Shen H, Ferrari M. Principles of nanoparticle design for overcoming biological barriers to drug delivery. *Nat Biotechnol.* 2015; 33:941–951. [PubMed: 26348965]
8. Rodriguez PL, Harada T, Christian DA, Pantano DA, Tsai RK, Discher DE. Minimal “Self” peptides that inhibit phagocytic clearance and enhance delivery of nanoparticles. *Science.* 2013; 339:971–975. [PubMed: 23430657]
9. Choi HS, Liu W, Misra P, Tanaka E, Zimmer JP, Ipe BI, Bawendi MG, Frangioni JV. Renal clearance of quantum dots. *Nat Biotechnol.* 2007; 25:1165–1170. [PubMed: 17891134]
10. Petros RA, DeSimone JM. Strategies in the design of nanoparticles for therapeutic applications. *Nat Rev Drug Discov.* 2010; 9:615–627. [PubMed: 20616808]
11. Wilhelm S, Tavares AJ, Dai Q, Ohta S, Audet J. Analysis of nanoparticle delivery to tumours. *Nat Rev Mater.* 2016; 1:16014.
12. Arami H, Khandhar A, Liggitt D, Krishnan KM. In vivo delivery, pharmacokinetics, biodistribution and toxicity of iron oxide nanoparticles. *Chem Soc Rev.* 2015; 44:8576–8607. [PubMed: 26390044]
13. Wang AZ, Langer R, Farokhzad OC. Nanoparticle delivery of cancer drugs. *Annu Rev Med.* 2012; 63:185–198. [PubMed: 21888516]
14. Huang HC, Barua S, Sharma G, Dey SK, Rege K. Inorganic nanoparticles for cancer imaging and therapy. *J Controlled Release.* 2011; 155:344–357.
15. Ghosh P, Han G, De M, Kim CK, Rotello VM. Gold nanoparticles in delivery applications. *Adv Drug Deliv Rev.* 2008; 60:1307–1315. [PubMed: 18555555]
16. Veisoh O, Tang BC, Whitehead KA, Anderson DG, Langer R. Managing diabetes with nanomedicine: challenges and opportunities. *Nat Rev Drug Discov.* 2014; 14:45–57. [PubMed: 25430866]
17. Dhar S, Daniel WL, Giljohann DA, Mirkin CA, Lippard SJ. Polyvalent Oligonucleotide Gold Nanoparticle Conjugates as Delivery Vehicles for Platinum(IV) Warheads. *J Am Chem Soc.* 2009; 131:14652–14653. [PubMed: 19778015]
18. Anselmo AC, Mitragotri S. A Review of Clinical Translation of Inorganic Nanoparticles. *AAPS J.* 2015; 17:1041–1054. [PubMed: 25956384]
19. Wilhelm S, Tavares A, Chan WCW. Reply to “Evaluation of nanomedicines: stick to the basics”. *Nat Rev Mater.* 2016; 1:16074.

20. Hirsch LR, Stafford RJ, Bankson JA, Sershen SR, Rivera B, Price RE, Hazle JD, Halas NJ, West JL. Nanoshell-mediated near-infrared thermal therapy of tumors under magnetic resonance guidance. *Proc Natl Acad Sci.* 2003; 100:13549–13554. [PubMed: 14597719]
21. Stern JM, Solomonov VVK, Sazykina E, Schwartz JA, Gad SC, Goodrich GP. Initial Evaluation of the Safety of Nanoshell-Directed Photothermal Therapy in the Treatment of Prostate Disease. *Int J Toxicol.* 2016; 35:38–46. [PubMed: 26296672]
22. Chen B, Li Y, Zhang X, Liu F, Liu Y, Ji M, Xiong F, Gu N. An efficient synthesis of ferumoxylol induced by alternating-current magnetic field. *Mater Lett.* 2016; 170:93–96.
23. Moran CH, Wainerdi SM, Cherukuri TK, Kittrell C, Wiley BJ, Nicholas NW, Curley SA, Kanzius JS, Cherukuri P. Size-dependent joule heating of gold nanoparticles using capacitively coupled radiofrequency fields. *Nano Res.* 2009; 2:400–405.
24. Henriksen-Lacey M, Carregal-Romero S, Liz-Marzán LM. Current Challenges toward In Vitro Cellular Validation of Inorganic Nanoparticles. *Bioconjugate Chem.* 2017; 28:212–221.
25. De Jong WH, Hagens WI, Krystek P, Burger MC, Sips AJ, Geertsma RE. Particle size-dependent organ distribution of gold nanoparticles after intravenous administration. *Biomaterials.* 2008; 29:1912–1919. [PubMed: 18242692]
26. Sykes EA, Chen J, Zheng G, Chan WCW. Investigating the Impact of Nanoparticle Size on Active and Passive Tumor Targeting Efficiency. *ACS Nano.* 2014; 8:5696–5706. [PubMed: 24821383]
27. Chiu YC, Gammon JM, Andorko JI, Tostanoski LH, Jewell CM. Modular Vaccine Design Using Carrier-Free Capsules Assembled from Polyionic Immune Signals. *ACS Biomater Sci Eng.* 2015; 1:1200–1205. [PubMed: 26689147]
28. Tietze R, Lyer S, Dürr S, Struffert T, Engelhorn T, Schwarz M, Eckert E, Göen T, Vasylyev S, Peukert W, Wiekhorst F, Trahms L, Dörfler A, Alexiou C. Efficient drug-delivery using magnetic nanoparticles-biodistribution and therapeutic effects in tumour bearing rabbits. *Nanomed Nanotechnol.* 2013; 9:961–971.
29. Arvizo RR, Miranda OR, Moyano DF, Walden CA, Giri K, Bhattacharya R, Robertson JD, Rotello VM, Reid JM, Mukherjee P. Modulating Pharmacokinetics, Tumor Uptake and Biodistribution by Engineered Nanoparticles. *PLoS One.* 2011; 6:e24374. [PubMed: 21931696]
30. Shah NB, Vercellotti GM, White JG, Fegan A, Wagner CR, Bischof JC. Blood–Nanoparticle Interactions and in Vivo Biodistribution: Impact of Surface PEG and Ligand Properties. *Mol Pharmaceutics.* 2012; 9:2146–2155.
31. Ernsting MJ, Murakami M, Roy A, Li SH. Factors Controlling the Pharmacokinetics, Biodistribution and Intratumoral Penetration of Nanoparticles. *J Control Release.* 2013; 172:782–794. [PubMed: 24075927]
32. Fischer H, Fournier-Bidoz S, Pang KS, Chan WCW. Quantitative detection of engineered nanoparticles in tissues and organs: An investigation of efficacy and linear dynamic ranges using ICP-AES. *NanoBiotechnology.* 2007; 3:46–54.
33. Kreyling WG, Abdelmonem AM, Ali Z, Alves F, Geiser M, Haberl N, Hartmann R, Hirn S, de Aberasturi DJ, Kantner K, Khadem-Saba G, Montenegro JM, Rejman J, Rojo T, de Larramendi IR, Ufartes R, Wenk A, Parak WJ. In vivo integrity of polymer-coated gold nanoparticles. *Nature Nanotechnol.* 2015; 10:619–624. [PubMed: 26076469]
34. Zhu ZJ, Tang R, Yeh YC, Miranda OR, Rotello VM, Vachet RW. Determination of the Intracellular Stability of Gold Nanoparticle Monolayers Using Mass Spectrometry. *Anal Chem.* 2012; 84:4321–4326. [PubMed: 22519403]
35. Elci SG, Yan B, Kim ST, Saha K, Jiang Y, Klemmer GA, Moyano DF, Tonga GY, Rotello VM, Vachet RW. Quantitative imaging of 2 nm monolayer-protected gold nanoparticle distributions in tissues using laser ablation inductively-coupled plasma mass spectrometry (LA-ICP-MS). *Analyst.* 2016; 141:2418–2425. [PubMed: 26979648]
36. Marsico A, Elci SG, Moyano DF, Tonga GY, Duncan B, Landis RF, Rotello VM, Vachet RW. Enhanced Laser Desorption/Ionization Mass Spectrometric Detection of Gold Nanoparticles in Biological Samples Using the Synergy between Added Matrix and the Gold Core. *Anal Chem.* 2015; 87:12145–12150. [PubMed: 26560844]

37. Yan B, Kim ST, Kim CS, Saha K, Moyano DF, Xing Y, Jiang Y, Roberts AL, Alfonso FS, Rotello VM, Vachet RW. Multiplexed Imaging of Nanoparticles in Tissues Using Laser Desorption/Ionization Mass Spectrometry. *J Am Chem Soc.* 2013; 135:12564–12567. [PubMed: 23931011]
38. Yeh YC, Saha K, Yan B, Miranda OR, Yu X, Rotello VM. The role of ligand coordination on the cytotoxicity of cationic quantum dots in HeLa cells. *Nanoscale.* 2013; 5:12140–12143. [PubMed: 24173625]
39. Chompoosor A, Saha K, Ghosh PS, Macarthy DJ, Miranda OR, Zhu ZJ, Arcaro KF, Rotello VM. The Role of Surface Functionality on Acute Cytotoxicity, ROS Generation and DNA Damage by Cationic Gold Nanoparticles. *Small.* 2010; 6:2246–2249. [PubMed: 20818619]
40. Ghosh PS, Verma A, Rotello VM. Binding and templation of nanoparticle receptors to peptide α -helices through surface recognition. *Chem Commun.* 2007:2796–2798.
41. Tang R, Moyano DF, Subramani C, Yan B, Jeoung E, Tonga GY, Duncan B, Yeh YC, Jiang Z, Kim C, Rotello VM. Rapid Coating of Surfaces with Functionalized Nanoparticles for Regulation of Cell Behavior. *Adv Mater.* 2014; 26:3310–3314. [PubMed: 24677290]
42. Liu J, Yu M, Zhou C, Zheng J. Renal clearable inorganic nanoparticles: a new frontier of bionanotechnology. *Materials Today.* 2013; 16:477–486.
43. Kumar R, Roy I, Ohulchanskyy TY, Vathy LA, Bergey EJ, Sajjad M, Prasad PN. In Vivo Biodistribution and Clearance Studies Using Multimodal Organically Modified Silica Nanoparticles. *ACS Nano.* 2010; 4:699–708. [PubMed: 20088598]
44. Zhang Y, Poon W, Tavares A, McGilvray ID, Chan WCW. Nanoparticle–liver interactions: Cellular uptake and hepatobiliary elimination. *J Control Release.* 2016; 240:332–348. [PubMed: 26774224]
45. Khlebtsov N, Dykman L. Biodistribution and toxicity of engineered gold nanoparticles: a review of in vitro and in vivo studies. *Chem Soc Rev.* 2011; 40:1647–1671. [PubMed: 21082078]
46. Brodie AE, Potter J, Reed DJ. Unique Characteristics of Rat Spleen Lymphocyte, L1210 Lymphoma and HeLa Cells in Glutathione Biosynthesis from Sulfur-Containing Amino Acids. *Eur J Biochem.* 1982; 123:159–164. [PubMed: 7067695]
47. Elci SG, Jiang Y, Yan B, Kim ST, Saha K, Moyano DF, Tonga GY, Jackson LC, Rotello VM, Vachet RW. Surface Charge Controls the Suborgan Biodistributions of Gold Nanoparticles. *ACS Nano.* 2016; 10:5536–5542. [PubMed: 27164169]
48. Mebius RE, Kraal G. Structure and function of the spleen. *Nat Rev Immunol.* 2005; 5:606–616. [PubMed: 16056254]
49. Thieblemont C, Rolland D, Baseggio L, Felman P, Gazzo S, Callet-Bauchu E, Traverse-Glehen A, Houlgatte R, Fu K, Weisenburger D, De Jong D, Jaffe ES, Rosenwald A, Ott G, Coiffier B, Berger F. Comprehensive analysis of GST- π expression in B-cell lymphomas: Correlation with histological subtypes and survival. *Leukemia & Lymphoma.* 2008; 49:1403–1406. [PubMed: 18604726]
50. Marucco A, Catalano F, Fenoglio I, Turci F, Martra G, Fubini B. Possible Chemical Source of Discrepancy between in Vitro and in Vivo Tests in Nanotoxicology Caused by Strong Adsorption of Buffer Components. *Chem Res Toxicol.* 2015; 28:87–91. [PubMed: 25564874]
51. Simons EJ, Bellas E, Lawlor MW, Kohane DS. Effect of Chemical Permeation Enhancers on Nerve Blockade. *Mol Pharmaceutics.* 2009; 6:265–273.

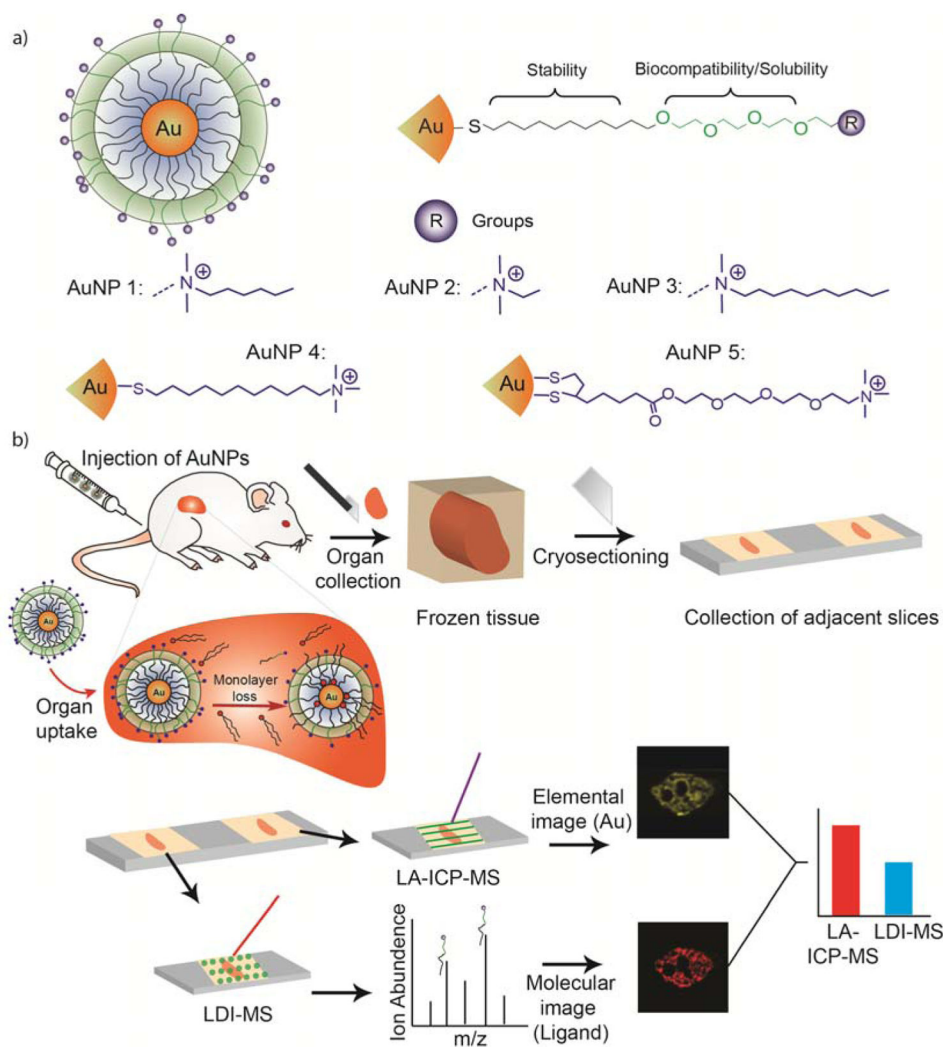
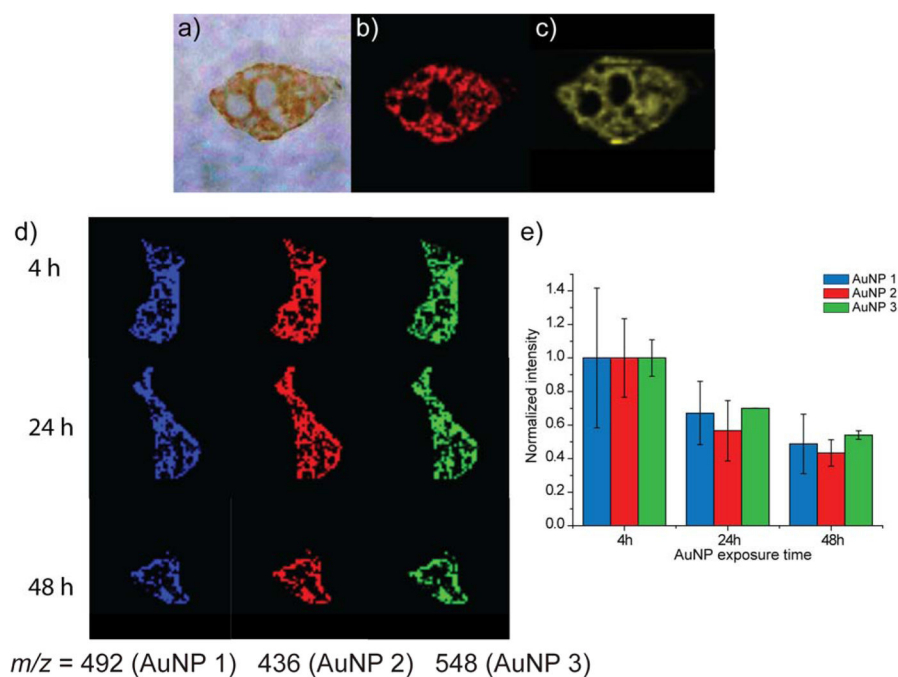


Figure 1. (a) Structure of the AuNPs used in this study. (b) Schematic representation of the experimental workflow.

**Figure 2.**

Comparison of the stability of AuNPs after 24 hours of injection in spleen slices from mice with AuNP 1. (a) Optical image of the spleen section. (b) LDI-MS image of AuNP 1 that reports on the monolayer signal for the spleen 24 h after injection, and (c) LA-ICP-MS image that reports on the Au signal for the spleen 24 h after injection. See the SI for instrument parameters and measurement details. (d) LDI-MS images of spleen slices at three different time points from mice injected with AuNP 1, AuNP 2, and AuNP 3. (e) Normalized LDI-MS intensities across the entire image for each AuNP, illustrating the loss of monolayer ligand signal over time. The approach for obtaining these normalized intensities, which accounts for differences in tissue slice sizes, can be found in the SI. Error bars represent variations in normalized intensities for images of multiple adjacent tissue slices (n=3).

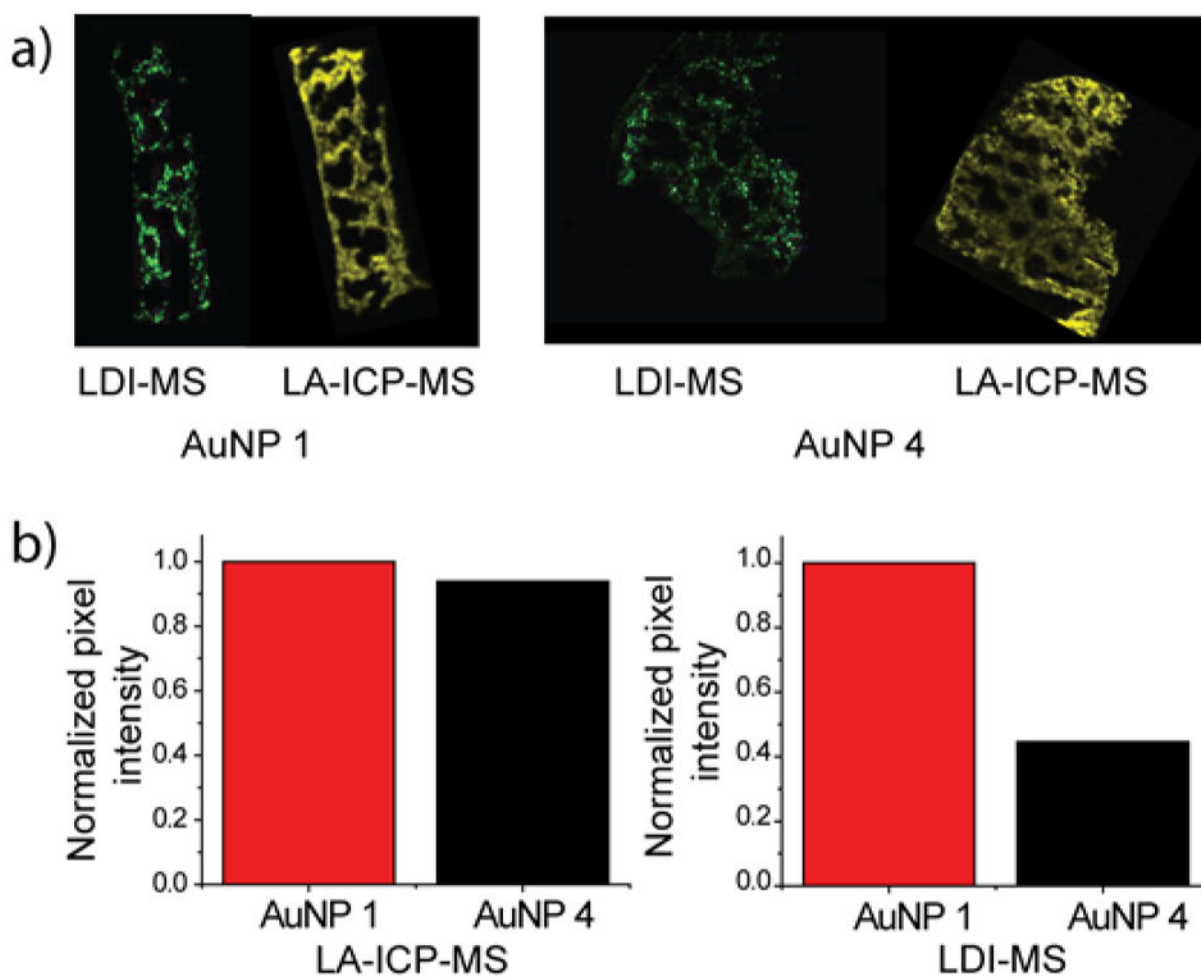


Figure 3. Comparison of the stability of AuNP 1 and AuNP 4 in the spleen 24 h after injection. (a) LDI-MS and LA-ICP-MS images showing the NP-bound monolayer and Au distributions, respectively, in the spleens of mice IV-injected with either AuNP 1 or AuNP 4. (b) Summed relative ion abundances of the Au and ligand ions from the LA-ICP-MS and LDI-MS images in (a). The normalized pixel intensity calculations are described in the SI.

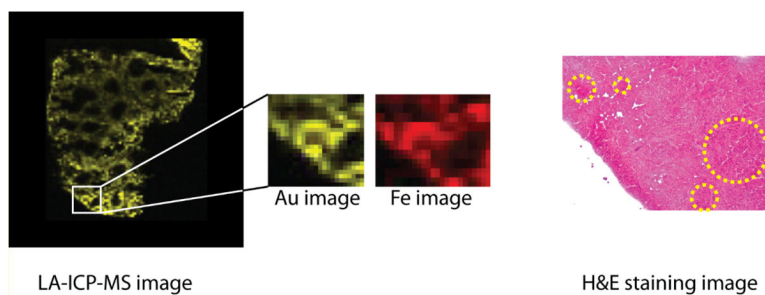


Figure 4. Example LA-ICP-MS and H&E staining images of a spleen tissue slice from a mouse injected with AuNP 4. The Fe image reflects the presence of the blood in the organ, distinguishing between the red pulp (higher Fe, red) and white pulp regions (lower Fe, black). The marginal zone is the interface between the red and white pulp regions and extends $\sim 40 \mu\text{m}$ from the white pulp. In the H&E stains, the pale pink color indicates the red pulp region, while the dark purple regions indicate the white pulp regions.

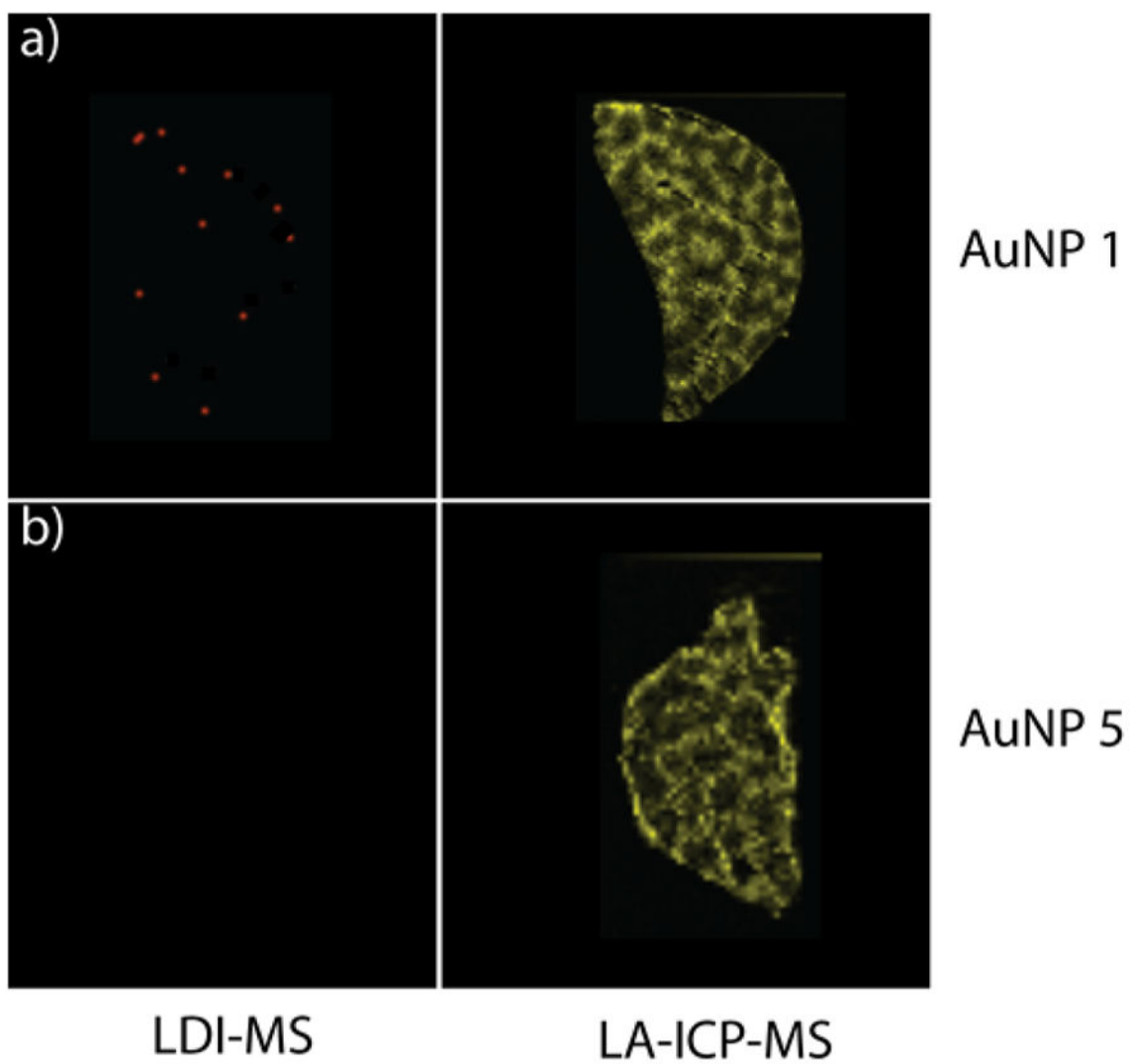


Figure 5. LDI-MS and LA-ICP-MS images of liver tissue slices from a mouse injected with (a) AuNP 1 and (b) AuNP 5 (24 h after injection).